Osteoarthritis and Cartilage 27 (2019) 1392–1402

Osteoarthritis and Cartilage

OARSI OSTEOARTHRITIS RESEARCH SOCIETY INTERNATIONAL

Propagation of microcracks in collagen networks of cartilage under mechanical loads

S. Santos †, N. Emery ‡, C.P. Neu §, D.M. Pierce † ‖ *

† Department of Biomedical Engineering, University of Connecticut, USA
‡ Department of Ecology and Evolutionary Biology, University of Colorado Boulder, USA
§ Department of Mechanical Engineering, University of Colorado Boulder, USA
‖ Department of Mechanical Engineering, University of Connecticut, USA

ARTICLE INFO

Article history:
Received 30 October 2018
Accepted 27 April 2019

Keywords:
Articular cartilage
Mechanical injury
Microcracks
SHG
Low-energy impact
Cyclic compression

SUMMARY

Objective: We recently demonstrated that low-energy mechanical impact to articular cartilage, usually considered non-injurious, can in fact cause microscale cracks (widths $< 30\ \mu m$) in the collagen network of visually pristine human cartilage. While research on macro-scale cracks in cartilage and microcracks in bone abounds, how *microcracks within cartilage* initiate and propagate remains unknown. We quantified the extent to which microcracks initiate and propagate in the collagen network during mechanical loading representative of normal activities.

Design: We tested 76 full-thickness, cylindrical osteochondral plugs. We imaged untreated specimens (pristine phase) via second harmonic generation and assigned specimens to three low-energy impact groups (none, low, high), and thereafter to three cyclic compression groups (none, low, high) which simulate walking. We re-imaged specimens in the post-impact and post-cyclic compression phases to identify and track microcracks.

Results: Microcracks in the network of collagen did not present in untreated controls but did initiate and propagate under mechanical treatments. We found that the length and width of microcracks increased from post-impact to post-cyclic compression in tracked microcracks, but neither depth nor angle presented statistically significant differences.

Conclusions: The microcracks we initiated under low-energy impact loading increased in length and width during subsequent cyclic compression that simulated walking. The extent of this propagation depended on the combination of impact and cyclic compression. More broadly, the initiation and propagation of microcracks may characterize pathogenesis of osteoarthritis, and may suggest therapeutic targets for future studies.

Introduction

Low-energy impacts to articular cartilage may initiate microcracks in the network of collagen,[1] which may be one of the earliest (i.e., pre-clinical) detrimental changes to cartilage. Such changes may contribute to osteoarthritis (OA), a leading cause of disability in adults. Clinical OA, characterized by the weakening and loss of cartilage, afflicts over 26.9 million people in the US alone,[2] leading to pain, disability, and total joint replacement. Following initiation of microcracks, repetitive mechanical loads to cartilage during normal daily activities may propagate these microcracks (within the extracellular matrix) and initiate the cascade of degeneration leading to OA. The extent of microcrack propagation during repetitive mechanical loads to cartilage during normal daily activities, however, is unknown.

The human knee is the largest joint in the body, and one of the most susceptible to injury.[3] Within the knee, acute or chronic damage may occur in the ligaments and tendons, as well as in the cartilage and bone, possibly resulting in post-traumatic osteoarthritis (OA).[4,5] While microcracks in bone have been characterized extensively,[6–10] and sub-millimeter-scale surface fissures in cartilage are well known for early to advanced osteoarthritis (OA), [11–14] we recently demonstrated that low-energy impact usually

* Address correspondence and reprint requests to: D.M. Pierce, Department of Mechanical Engineering, University of Connecticut, 191 Auditorium Road, Unit 3139 Storrs, CT 06269-3139, USA.
E-mail address: dmpierce@engr.uconn.edu (D.M. Pierce).

https://doi.org/10.1016/j.joca.2019.04.017
1063-4584/

considered non-injurious can in fact cause micrometer-scale cracks (microcracks) in the collagen network of human cartilage.[1] In previous work we defined collagen-network microcracks as fractures in the collagen network that are no wider than the diameter of chondrocyte lacunae ($< 30\ \mu$m). [15,16] Furthermore, we probed the diminished functional response of cartilage under progressive cyclic loading[17] and found statistically significant microcracking under some loading conditions.

Using second harmonic generation imaging (SHG) via confocal microscopy, we previously visualized micro-scale mechanical damage to the network of collagen that we initiated from low-energy impact. Other researchers applied compression,[18] tension,[19] or surgically induced injury[20] and used 2-D or 3-D SHG visualize (but never quantify) microcracks in the network of collagen (referred to as microcracks, micro-splits, and micro-wrinkles). Microcracks also present *in vivo*, as seen by us and others, e.g., in mice with surgically induced OA[20] and in ICRS Grade-I human femoral cartilage.[21]

In this study, we aimed to determine: (1) what combinations of impact and cyclic compression initiate microcracks in the network of collagen; and (2) whether and how cartilage microcracks propagate during cyclic, mechanical loading which simulates walking. Understanding these aims contributes understanding to the initial mechanisms of microscale damage in the network of collagen that may be a precursor to degradation characteristic of OA.

To these ends, we initiated microcracks in the network of collagen in cartilage explants using low-energy mechanical impacts, and tracked the propagation of microcracks after cyclic compression simulating 12,000 walking strides, approximately equivalent to completing a half marathon paced at 13–15 min per mile.[22] Using SHG microscopy, we measured microcrack area density before and after impact and after cyclic loading, and quantified changes in microcrack morphology (length, width, and depth) and orientation.

Materials and methods

In total we tested 76 full-thickness, cylindrical osteochondral plugs (specimens). We separated specimens from the lateral and medial femoral condyles, and assigned them to one of three different impact groups (none, low, high), with impact energy density as the independent variable, and thereafter one of three different cyclic compression groups (none, low, high) which simulate 12,000 walking strides. We also performed SHG imaging (Carl Zeiss LSM 510 or Nikon FN1) at three experimental phases (pristine, post-impact, and post-cyclic compression). In Fig. 1 we show a summary of the treatment groups. In total, we had seven different treatment groups, where one control group received neither impact nor cyclic compression, two control groups received only cyclic compression, and the remaining four groups received both impact and cyclic compression.

Preparation of specimens

We received full bovine knees from five skeletally mature animals (18–30 months) packed on ice (Animal Technologies, Inc., Tyler, TX). We carefully exposed and identified load-bearing and visibly pristine regions on both the lateral and medial femoral condyles, and determined the local split-line direction along these surfaces.[23,24] We then extracted cylindrical specimens (3 mm diameter, full thickness) using a circular punch while keeping track of the local split-line direction. Using a scalpel, we removed a majority of the subchondral bone while ensuring that the remaining subchondral bone surface was visibly parallel to the articular surface. Using a digital camera (EOS 70D DSLR; Canon, Tokyo, JP), we imaged each cylindrical specimen and used standard image processing to determine the thickness of cartilage.[25] To store specimens not immediately tested, we immersed them in Phosphate Buffered Saline (PBS, pH 7.4) and stored them at −80°C.[23,26] On the day of testing we thawed the specimens and mounted them to custom, ultra-wear-resistant nylon platens using cyanoacrylate adhesive for subsequent imaging and mechanical testing.

Mechanical tests

Low-energy impact

We impacted the articular surface of unconfined pristine specimens using a custom drop tower with a polished, flat metal impactor (diameter much greater than 3 mm). We separated specimens from the lateral and medial femoral condyles and randomly assigned those specimens to three different impact groups (no impact-*NI*, low impact-*LI*, high impact-*HI*). Based on preliminary studies, we selected *LI* = 1.5–2.5 mJ/mm^3 and *HI* = 2.5–4.0 mJ/mm^3. Based on our previous work,[1] we selected the intended impact velocity $v^*_{\text{imp}} = 0.5$ m/s. We calculated the required drop height $h = (v^*_{\text{imp}})^2/2g$, with g as gravitational acceleration. We then calculated the required total drop mass m to achieve the intended impact energy density E^*_{imp} using

$$E^*_{\text{imp}} = \frac{mgh}{V}, \tag{1}$$

where V is the volume of the specimen.

During the test we measured the acceleration (±49,000 m/s^2; 350A14, PCB Piezotronics, Depew, NY) and the force (22.24 kN; 200B05, PCB Piezotronics) at 100,000 Hz sampling rate. After the test, we integrated the acceleration once to determine the actual velocity at the moment of impact v_{imp}, and used this to calculate the actual the impact energy density (E_{imp}) applied to each specimen using

$$E_{\text{imp}} = \frac{mv^2_{\text{imp}}}{2V}. \tag{2}$$

For the control group (*NI* in Fig. 1), specimens rested in PBS for the duration of the test. Post-impact, we submerged the specimens

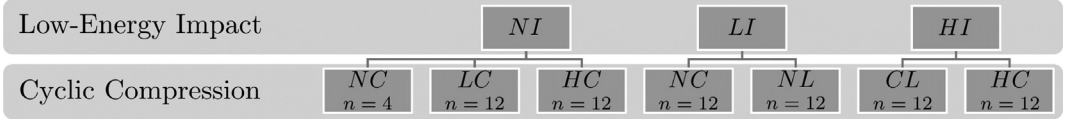

Fig. 1. Summary of 76 specimens separated into treatment groups, with specimens from the medial and lateral condyles pooled together. Low-Energy Impact: no impact–*NI*, low impact–*LI* (1.5–2.5 mJ/mm^3), high impact–*HI* (2.6–4.0 mJ/mm^3). Cyclic Compression: no compression–*NC*, low compression–*LC* (10%), high compression–*HC* (15%).

in PBS at 37°C for at least 1 h to equilibrate prior to subsequent imaging and mechanical testing.[1]

Cyclic, unconfined compression

Post-impact, we conducted unconfined cyclic compression tests, a technique well-established in the literature,[27–29] using a Bose LM1 Electroforce linear motor with WinTest 7 soft,ware (Bose, Eden Praire, MN). First, we submerged the tissue in PBS solution at 37°C and maintained force-controlled 0.2 N compression for 3,000 s. We then applied a pattern of cyclic compression including 0.69 s sinusoidal compression followed by 0.67 s recovery (total cycle time equals 1.36 s or 0.74 hz), cf. Zhang *et al.*[30] The amplitude of cyclic compression was either low compression – $LC = 10\%$ or high compression – $HC = 15\%$ of the cartilage thickness measured prior to impact testing, cf. Liu *et al.*,[31] Harkey *et al.*.[32] For the control group (high compression – *NC* in Fig. 1), specimens rested in PBS for the duration of the test. Post-cyclic compression, we submerged the specimens in PBS at 37°C for at least 1 h prior to subsequent imaging.[1]

Images via second harmonic generation (SHG)

We performed SHG imaging (Zeiss LSM 510, Oberkochen, DE or Nikon FN1, Tokyo, JP) at three separate experimental phases (pristine–*P*, post-impact–*PI*, and post-cyclic compression–*PC*). We used tunable Ti: Sapphire lasers (Zeiss: Coherent Chameleon, Santa Clara, CA or Nikon: Spectra Physics, Santa Clara, CA) at 850 nm for excitation of the nonlinear signal. We acquired the signals in non-descanned detection using a specialized filter (Zeiss: 425 ± 13 nm bandpass filter; FF01-425/26-25, Semrock, Rochester, NY or Nikon: 492 blocking edge short pass filter; FF01-492/SP-25, Semrock). For all images from the Zeiss, we used a water-immersion objective (W Plan-Apochromat 20×/1.0) and a 600 × 600 μm (512× 512 pixel) field of view. For all images from the Nikon, we used a water-immersion objective (CFI75 Apochromat LWD 25× MP) and a 516 × 516 μm (1024 × 1024 pixel) field of view. For each specimen, we acquired a 7 × 7 tile grid (100 μm tile overlap) of the entire articular surface at three separate experimental phases (*pristine (P)*, *post impact (PI)*, and *post-cyclic compression (PC)*). Additionally, both PI and PC we acquired through-thickness image stacks (slice increment of 2.5 μm) from a 3 × 3 tile grid centered on the articular surface (to avoid edge effects). We acquired image stacks 50 μm into the specimen measured from the articular surface and scanned for microcracks. We stopped imaging if we found no microcracks. If we identified microcracks, we continued imaging up to 200 μm into the specimen (the approximate focal length of the microscopes). We also mounted each specimen to keep the placement, and thus orientation of the images with respect to the split-line direction, consistent.

Analyses of images

We stitched together our SHG images using Fiji's Grid/Collection Stitching Plugin[33] for ImageJ (National Institutes of Health, Bethesda, MD) to generate images of the full circular cross section at a resolution of 1.2 μm/pixel (Zeiss) or 0.50 μm/pixel (Nikon). In SHG, collagen fibers/fibrils create the strongest SHG signals.[34] The collagen signal was white (Zeiss) or blue (Nikon), and we identified microcracks as absence of SHG signal (black).[1,34] Using only the 3 × 3 tile grid centered on the articular surface (Zeiss: 3618.8 × 3618.8 μm, 3093 × 3093 pixels; Nikon: 3092.5 × 3092.5 μm, 6185 × 6185 pixels), independent observers measured the length, width, and principal angle (relative to the split-line direction) of each microcrack in each image (parallel to the articular surface) manually, using the measurement tools in Fiji. To determine the microcrack depth, each observer first determined the height of the articular surface (defined as the axial position when 50% of surface was visible/non-black in each individual image, and then followed each microcrack axially through the image stacks (slice interval of 2.5 μm) until each disappeared. We recorded these data overall in the pristine, post-impact, and post-cyclic compression phases of the experiment. Additionally, where we could positively track individual microcracks by feature matching from the post-impact to the post-cyclic compression phases of the experiments, we recorded the specific morphology and orientation of each tracked microcrack as a subset of the overall data.

To validate inter-observer agreement in our measured data, we calculated the Cohen's kappa coefficient κ, a 95% confidence interval, and the inter-rater reliability using SAS 9.4 (SAS Institute, Inc., Cary, NC). We also verified inter-observer reliability by comparing the means using a *t*-test with $p < 0.05$ to determine significant differences among observers. If we found agreements greater than 75% from two independent observers, we averaged these results.[35,36] If we found practically significant differences between observers, we included a third independent observer and averaged the two sets of results with the best inter-observer agreement (always greater than 75%).

We calculated the length, width, depth, and orientation (angle from the split-line direction) of all microcracks from both post-impact and post-cyclic compression phases. For each specimen, we also calculated the overall microcrack area density using the total number of microcracks in the 3 × 3 tile grid centered on the articular surface.

Statistical analyses

We used separate mixed-model ANOVAs to evaluate the effects of impact and cyclic compression on microcrack density, and on the length, width, depth, and angle of microcracks. We included condyle (medial or lateral), impact level (low or high), cyclic compression level (10% or 15%), and phase (PI or PC) as fixed effects, specimen as a random effect, and the thickness of each cartilage specimen as a covariate. We also included all two-way interactions between impact, cyclic compression, and phase, as well as the interaction between sample thickness and impact level. Prior to analysis, we $\log(x+1)$ transformed mean microcrack density, width, and depth, and $\sqrt{(x+1)}$ transformed mean microcrack length, to meet the assumptions of ANOVA. Even after transformation, the data for mean microcrack length failed to meet the assumption of normality of residuals due to two outliers. We tested if the outliers were driving our results for mean microcrack length by running the model with and without the outliers included. Removing the outliers did not alter the significance of any variables in the model; for brevity, we present only the results of the analysis using the full data set (including the outliers). We used *post-hoc* tests to evaluate differences among treatment combinations for any statistically significant interactions between fixed effects. Finally, we used separate simple regressions to investigate interactions that we identified as statistically significant between specimen thickness and each impact level for mean microcrack width. This involved generating the residuals from a reduced, mixed-model ANOVA that did not include thickness or the thickness × impact level interaction,

and then testing for a statistically significant relationship between specimen thickness and the residual mean microcrack thickness for each impact level.

We analyzed the subset of our data where we tracked individual cartilage microcracks over the course of the experiment using the same mixed-model ANOVA, but with specimen and microcrack included as additional random factors (to account for non-independence at those scales), and the three-way interaction among impact, cyclic compression, and phase. Prior to analysis, we $\log(x+1)$ transformed mean length, width, and depth of the tracked microcracks to meet the assumptions of ANOVA. Data for the orientation of the tracked microcracks met the assumptions of ANOVA without transformation.

Results

We completed mechanical treatments and imaging on a total of 76 specimens including controls (*NI, NC* in Fig. 1). We did not find any microcracks in the untreated controls. We found no statistically significant differences between lateral and medial condyles, so we pooled data from these two groups to increase our statistical power. We successfully initiated microcracks in verified, visibly pristine cartilage, and propagated the microcracks under cyclic compression (Fig. 2).

We found statistically significant differences in the density, length, width, depth, and angle of microcracks depending on the combinations of mechanical treatments (Table I, Appendix (A) and Table II, Appendix (B)). We found no microcracks in any of our control specimens (column *NI* in Table I), nor any microcracks in our pristine specimens prior to impact treatments (row *P*).

Under our loading combinations, we found that when microcracks form, they most likely present with the following morphologies: lengths $<40\,\mu$m, widths $<20\,\mu$m, depths $<30\,\mu$m, and angles either 0° or 45° to the split-line direction (Fig. 6, Appendix (C)).

Microcrack initiation

We initiated microcracks during low-energy impacts, and both initiated and propagated microcracks during unconfined cyclic compressions. We found no statistically significant differences in median microcrack densities, lengths, or depths in our controls, and under our combinations of impact and cyclic-compression treatments (Fig. 3). We did find statistically significant larger median angles (from split-line direction) of microcracks in specimens from the high-impact compared to the low-impact treatment group at 15% cyclic compression ($P = 0.0252$).

Median microcrack widths were: (1) larger for those initiated at high impacts than for those initiated at low impacts overall ($P = 0.0213$).

(2) larger for those initiated at high impacts than for those initiated at low impacts and subsequently undergoing 10% cyclic compression ($P = 0.0252$), and (3) smaller for those undergoing 10% as compared to 15% cyclic compression after high impacts ($P = 0.0398$) (Fig. 4). We found that log microcrack width correlated with cartilage thickness under high ($\log(W+1) = 0.983T + 1.23$, $P = 0.0025$) but not low impacts.

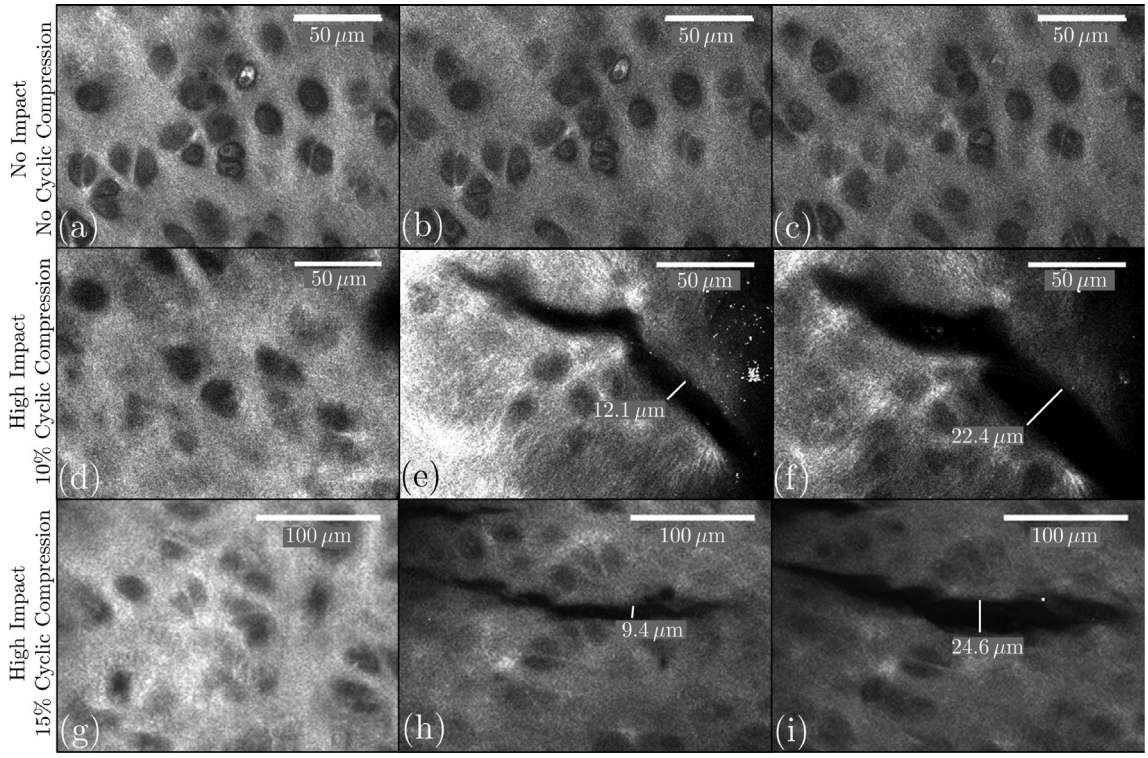

Fig. 2. Representative second harmonic generation imaging (SHG) images of a control specimen (a–c) resting in PBS for the duration of the mechanical tests, and of two mechanically treated specimens (d–i) presenting microcracks: (d, g) pristine (P); (e, h) post impact (PI) at 2.5–4.0 mJ/mm^3; and (f, i) post-cyclic compression (PC) at 10% and 15% respectively. We co-registered images for each specimen using relative coordinate mapping and feature matching.

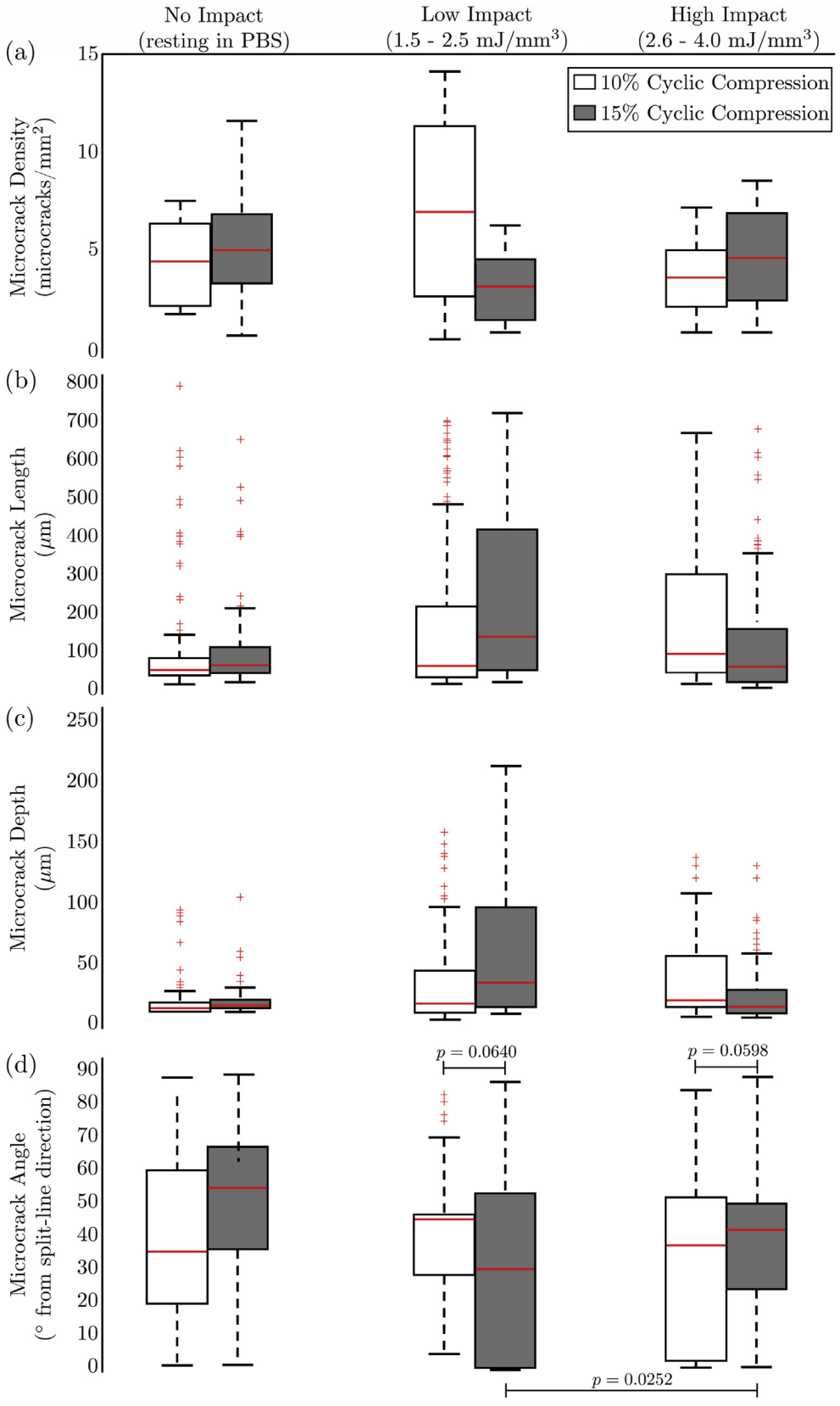

Fig. 3. There are no statistically significant differences in densities, lengths, or depths of cartilage microcracks under different combinations of impact and cyclic compression treatments. Plot shows distributions in (a) density, (b) length, (c) depth, and (d) angle (from the split-line direction) of cartilage microcracks observed after no impact (left column), low impact (middle column), or high impact (right column) and one of two cyclic compression treatments. Control specimens (no impact/no cyclic compression) presented no microcracks in any specimens (not shown). Here we show raw data. We determined statistical significance using mixed-model ANOVAs for each response variable. We transformed these data prior to analyses as described in Section Statistical analyses.

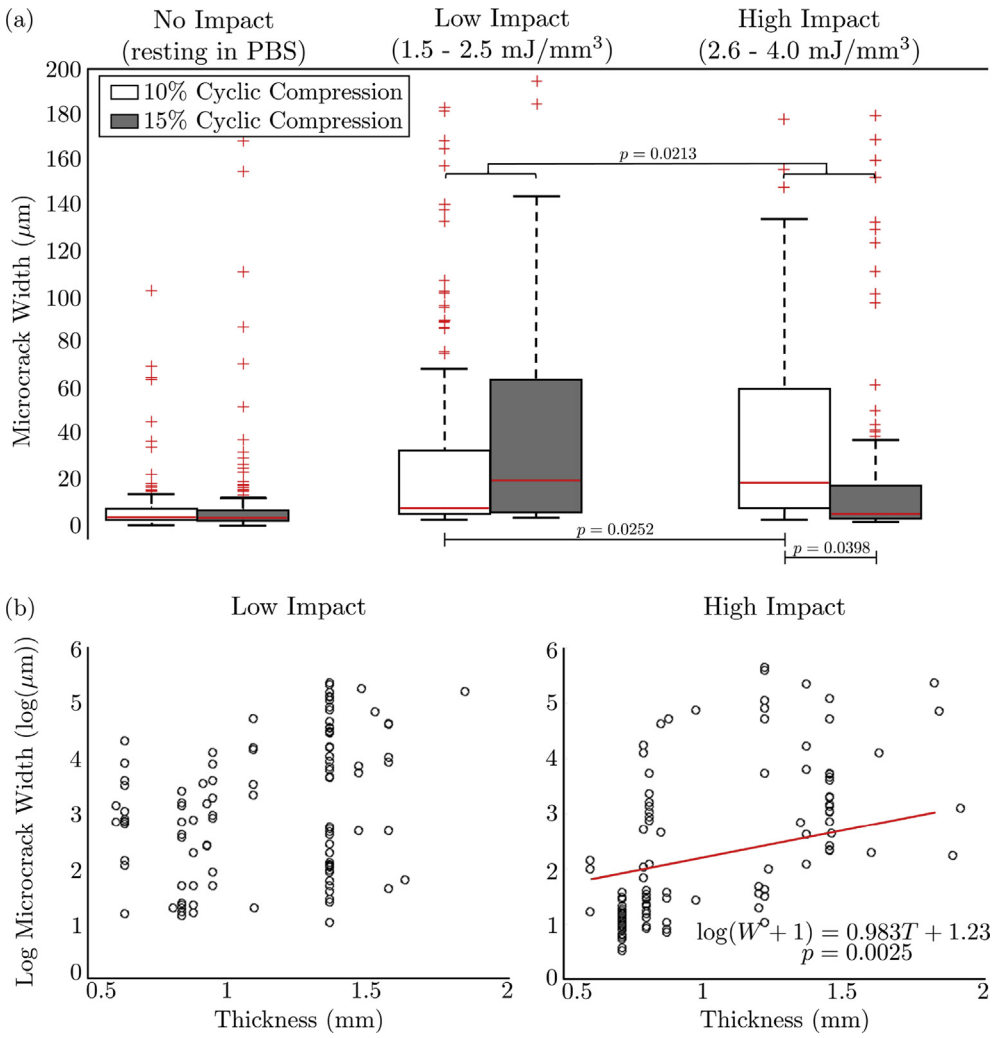

Fig. 4. We found statistically significant, large differences in widths of cartilage microcracks under different combinations of impact and cyclic compression treatments (see Table II for statistical results). Plot (a) shows distributions in width of cartilage microcracks observed after no impact (left column), low impact (middle column), or high impact (right column) and one of two cyclic compression treatments. Control specimens (no impact/no cyclic compression) presented no microcracks in any specimens (not shown). Plot (b) shows log microcrack width vs cartilage thickness for both low and high impact treatments. Here we show raw data unless indicated otherwise. We determined statistical significance using mixed-model ANOVAs with 47 degrees of freedom for each response variable. We transformed these data prior to analyses as described in Section Statistical analyses.

Microcrack propagation

In tracked microcracks, the main effect of phase (post-impact vs post-cyclic compression) showed microcrack lengths and widths measured post cyclic compression were statistically significantly greater than those measured post impact ($P < 0.0001$). Regarding length specifically, the interaction between level of cyclic-compression and level of impact was also statistically significant ($P = 0.018$), but we did not pursue this with *post-hoc* tests. Regarding the width of tracked microcracks, two interactions with impact level were significantly different in our *post-hoc* tests: impact × cyclic compression ($P = 0.025$) and impact × phase ($P = 0.043$). To further probe these interactions, we ran separate models for each impact (thus dropping terms or interactions containing impact). These analyses found that after high impact, widths grew from the post-impact phase to the post-cyclic compression phase. Additionally, we found statistically significantly larger widths after 10% cyclic compression than after 15%, but only in the low-impact treatment group (Fig. 5).

We found no statistically significant differences in the depth of tracked cartilage microcracks between post impact and post-cyclic compression, but did find different combinations of impact and cyclic compression influenced the microcrack depth ($P = 0.014$). Similarly, we did not see statistically significant changes in microcrack angle (with respect to the split-line direction) from post impact to post-cyclic compression, but did find different combinations of impact and cyclic compression influenced the angle of microcracks ($P = 0.020$).

Discussion

Regular mechanical loading is one of the most important environmental factors in maintaining cartilage and joint health, but severe loading can also have degradative effects that

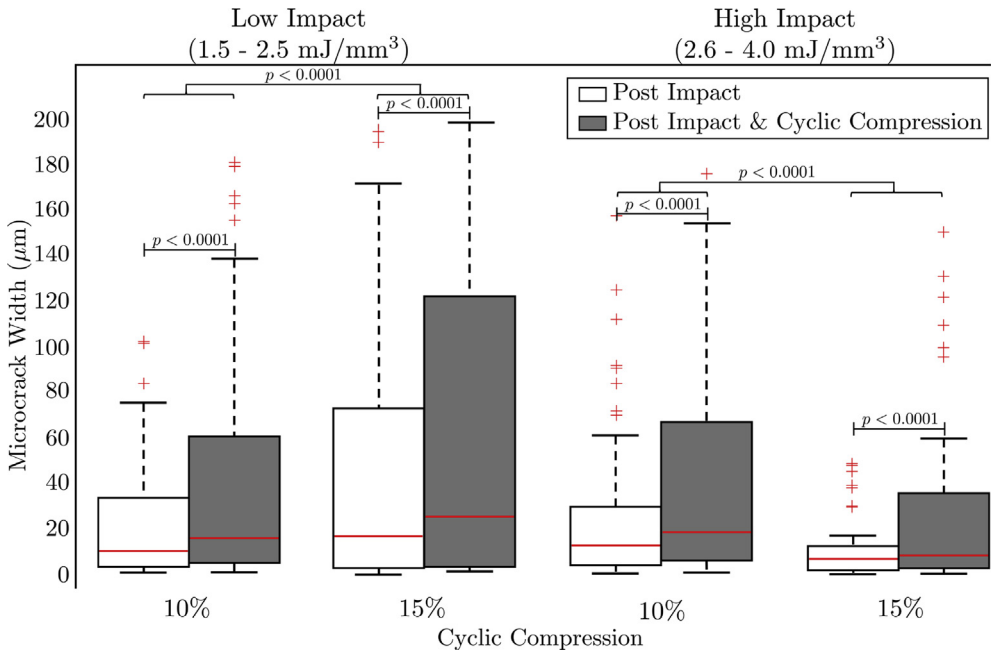

Fig. 5. Cartilage microcracks propagate from post-impact to post-cyclic compression phases of mechanical treatments. Plot shows distributions of widths of tracked cartilage microcracks under four combinations of impact and cyclic compression treatments. Control specimens (cyclic compression with no impact) presented no tracked microcracks in any specimens (not shown). Here we show raw data. We transformed these data prior to analyses as described in Section Statistical analyses.

influence the development of OA.[4] Because cartilage undergoes various combinations of mechanical loading *in vivo*, mechanical analyses of cartilage should employ similarly complex loading treatments.

We were the first to successfully identify and track progression of individual microcracks in the collagen networks of cartilage under *in vitro* mechanical loading while maintaining the full thickness of cartilage. In this study we determined combinations of impact and cyclic compression that affect the propagation of microcracks.

In articular cartilage, covalent cross-links among fibrils and fibers stabilize the network of collagen.[37] These cross-links predominantly connect telopeptides of adjacent molecules.[38] There are several damage mechanisms within articular cartilage that may contribute to OA, including breaking[39,40] and peeling of collagen fibrils.[41] Bonitsky *et al.*[42] found they could not repair (macro-scale) fissures with cross-linking treatments. Given the significance of damage to the collagen network within cartilage, understanding the initiation and propagation of microcracks could provide essential insight into the initiation of OA.

Microcrack initiation

We initiated microcracks using relatively low impact energy densities of 1.5 – 4 mJ/mm^3 (approximately 0.042 – 0.11 J) given the average dimensions of our specimens. Rapid impact loading leads to tensile stresses within the collagen fibers and renders them susceptible to rupture.[43] Larger impact energies yielded microcracks with overall greater initial microcrack widths. Duda *et al.*[14] impacted fully intact porcine patella with comparably low impact energies (0.06 – 0.2 J) and did not find fissures using electron microscopy, but did find damage to chondrocytes. Using SHG, we were able to see microcracks in the network of collagen at comparable (or lower) impact energies. These differences may be due to differences in experimental design, species and/or location of tissue, and/or imaging modality. In some cases, we also initiated microcracks during cyclic compression. Larger tensile stresses within the compromised collagen network may then cause the formation of new microcracks.[5]

Based on preliminary studies, we initiated our microcracks at an impact velocity of 0.5 m/s. Kaleem *et al.*[1] initiated cartilage microcracks with impact velocities ranging from 0.75 m/s to 1.0 m/s and impact energies in the range of 0.05 – 0.09 J, but did not include cyclic compression among their mechanical treatments. With these impact treatments, they determined that impact energy densities of approximately 1.5 – 3 mJ/mm^3 initiate microcracks in human cartilage, and that increasing impact velocity did not correlate with increasing occurrence of microcracks.

We found that cartilage microcracks can form at various angles ranging from parallel to perpendicular to the split-line direction; however the majority of microcracks tended to form either parallel to the split-line direction or at 45° to it. Microcracks forming parallel to the split-line direction may indicate voids between aligned collagen fibers forming as cross-links rupture.[37] Cartilage microcracks forming at 45° to the split-line direction may indicate rupture of both cross-links and collagen fibers.

We found that cartilage thickness significantly correlated with median width of initiated microcracks for high (1.5 – 2.5 mJ/mm^3) but not low (2.5 – 4.0 mJ/mm^3) impacts [Fig. 4(b)], i.e., specimens with greater thicknesses generate microcracks with greater initial widths. In previous research we found that other mechanical responses of cartilage correlate with thickness, e.g., energy dissipation under shear deformations decreased with increased cartilage thickness.[44]

Microcrack propagation

In several instances while tracking microcracks, we identified microcracks in the post-impact phase but could no longer find them in the same locations in the post-cyclic compression phase. Post high impact, we also found that microcrack widths grew less after subsequent 15% cyclic compression than after 10% cyclic compression. Since we did not use living cartilage for these experiments, these microcracks likely closed or fused by readjustment of the extra-cellular matrix under cyclic compression. Many studies demonstrate that the collagen network within cartilage realigns during cyclic loading.[14,45] Brown *et al.*[46] suggest that collagen fibers bundle near the cartilage surface after damage to the network of collagen, and that such bundles are visible via SHG as brighter white lines. We did see bright white lines near the cartilage surface, perhaps resulting from fiber realignment to create fiber bundles. Such realignment within the extra-cellular matrix may account for our disappearing microcracks.

Limitations and outlook

We used 3 mm diameter plugs, which may not represent *in vivo* conditions[11]. This study serves as a first investigation into the propagation of microcracking, and correlations to conditions *in vivo* require further experiments. We found small cartilage microcracks near the edges of the cut cylindrical surfaces in several pristine

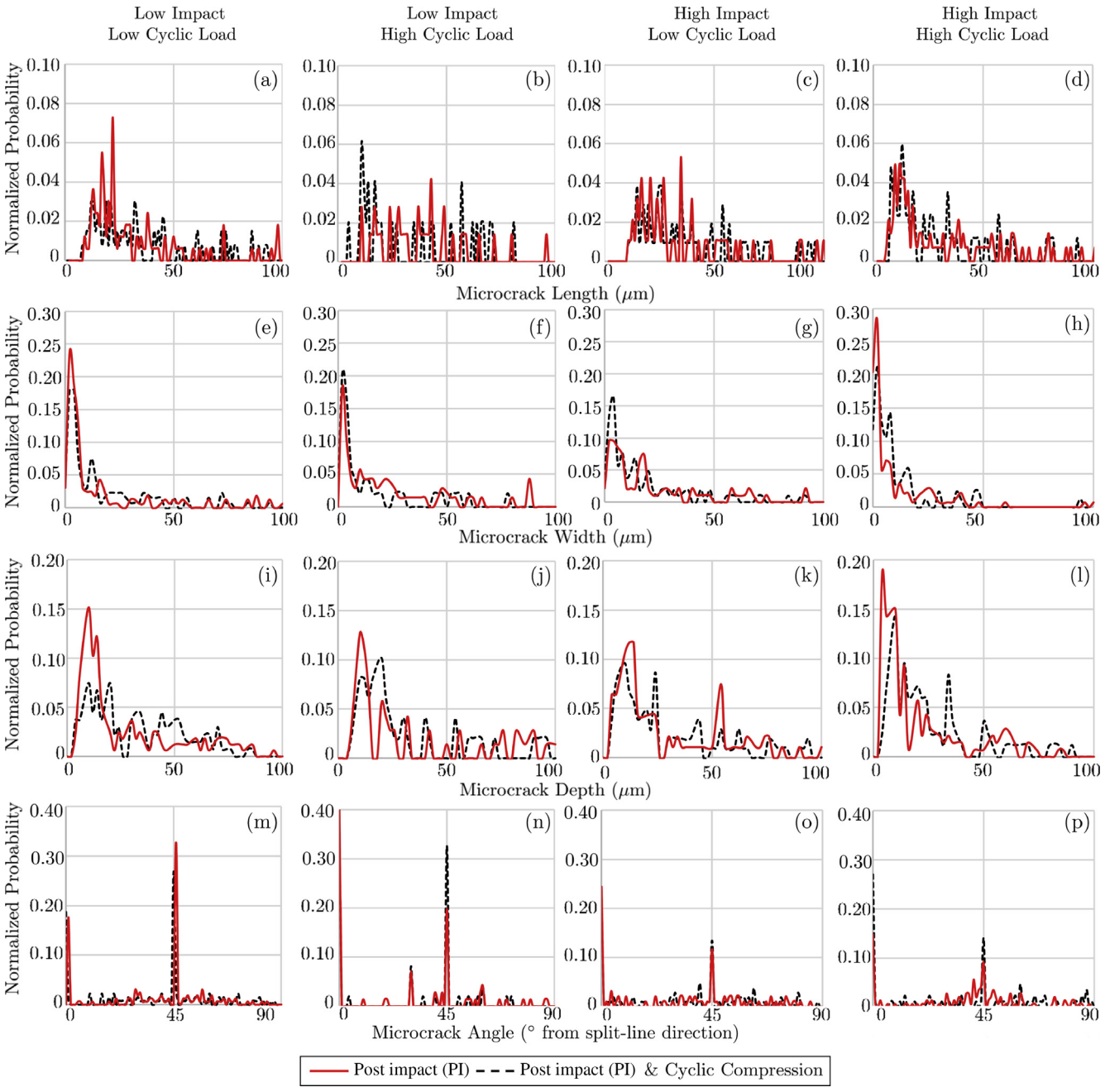

Fig. 6. Normalized probability of finding microcracks at given lengths (a–d), widths (e–h), depths (i–l), and angles with respect to the split-line direction (m–p). The solid red line in each figure represents data PI, while the black dashed line represents data post-cyclic compression.

specimens, these resulting from extraction of our specimens. Some of these microcracks propagated towards the center of the explants, likely influencing the integrity of the collagen network during our mechanical treatments. During imaging we considered only the center region of our explants to (largely) avoid including these microcracks in our analyses, but they may have influenced propagation of surrounding microcracks initiated during our mechanical treatments.

Post-traumatic osteoarthritis (PTOA) involves mechanical insult and an inflammatory cascade. In previous studies using SHG, we screened cartilage from total knee arthroplasties (TKAs) and found microcracks occurring naturally in human cartilage with very early-stage OA. Similarly, Kumar *et al.*[21] identified, via SHG imaging, cartilage microcracks (which they called microsplits and wrinkles) in very early-stage OA (ICRS Grade-I) femoral cartilage from TKAs. OA involves biomechanical, biochemical, metabolic, and genetic changes often triggered by injury and inflammation pathways.[47,48] Future studies aimed at understanding the interplay of mechanical and cellular mechanisms in cartilage microcracks, e.g., connecting microcrack propagation *in vivo* and marathon running,[49] may enable new treatment targets and detection of pre-clinical/early OA.[50]

In summary, our results show: (1) changes in overall microcrack width significantly depend on loading conditions where greater propagation occurs after low impacts; and (2) microcracks propagate by increasing in both length and width, but not depth. The microcracks we initiated under low-energy impact loading increased in length and width during subsequent cyclic compression that simulated walking. The extent of this propagation depended on the combination of impact and cyclic compression. More broadly, the initiation and propagation of microcracks may characterize pathogenesis of osteoarthritis, and may suggest therapeutic targets for future studies.

Author contributions

SS contributed to conception and design; prepared specimens and conducted the experiments; analyzed and interpreted data; participated in drafting the article and revising it critically; and gave final approval of the version submitted. NE analyzed and interpreted data; participated in drafting the article and revising it critically; and gave final approval of the version submitted. CPN analyzed and interpreted data; participated in drafting the article and revising it critically; and gave final approval of the version submitted. DMP oversaw the project; contributed to conception and design; analyzed and interpreted data; participated in drafting the article and revising it critically; and gave final approval of the version submitted.

Conflict of interest statement

We have no conflicts of interest to report.

Role of the funding source

The National Science Foundation and the Ford Fellowship Foundation had no involvement in the study design; in collection, analysis and interpretation of data; in the writing of the manuscript; or in the decision to submit the manuscript for publication. Any opinions, findings, and conclusions or recommendations expressed in this material are those of the author(s) and do not necessarily reflect the views of the National Science Foundation.

Acknowledgments

This material is based upon work supported by the National Science Foundation under Grant Number (CAREER 1662429) and the Ford Fellowship Foundation. We thank undergraduate research assistants Maria Antony, Victoria Blair, Lauren Contenta, Jenna Clum-Russell, Gina DiGiacomo, Jacob Grosso, Zinnia Hall, Hannah Kackley, Emilio Loren de Mola, Kathryn Morozov, Jennifer Pires, Bryanna Samolyk, Brian Tassavor, and Paige Woods for assistance with imaging and analyses. We also thank Chris O'Connell (University of Connecticut, Storrs) for assistance with the Zeiss LSM 510 and James Chambers (University of Massachusetts, Amherst) for assistance with the Nikon FN1.

Appendix A

In Table I we present the medians and interquartile ranges of the lengths, widths, depths, and angles of microcracks in the pristine, PI, and post-cyclic compression phases of our experiment under one of three different impact treatments (none, low, high), and thereafter one of three different cyclic compression treatments (none, low, high).

Table I
Plots show the medians and interquartile ranges [Q_1, Q_3] of the lengths, widths, depths, and angles of microcracks in the pristine (*P*), post impact (*PI*), and post-cyclic compression (*PC*) phases of our experiment under the three different impact treatments (no impact–*NI*, low impact–*LI* (1.5–2.5 mJ/mm^3), and high impact–*HI* (2.6–4.0 mJ/mm^3)) and thereafter the three different cyclic compression treatments (no compression–*NC*, low compression–*LC* (10%), and high compression–*HC* (15%)).

		NI			*LI*		*HI*	
		NC	*LC*	*HC*	*LC*	*HC*	*LC*	*HC*
P	Density (#/μm^2)	0.0	0.0	0.0	0.0	0.0	0.0	0.0
	Length (μm)	0.0	0.0	0.0	0.0	0.0	0.0	0.0
	Width (μm)	0.0	0.0	0.0	0.0	0.0	0.0	0.0
	Depth (μm)	0.0	0.0	0.0	0.0	0.0	0.0	0.0
	Angle ($^\circ$)	0.0	0.0	0.0	0.0	0.0	0.0	0.0
PI	Density (#/μm^2)	0.0	–	–	3.9 [1.6,5.4]	0.78 [0.39,2.2]	4.0 [2.0,4.9]	2.5 [1.5,3.8]
	Length (μm)	0.0	–	–	48.7 [26.9,109.3]	126.7 [37.2,351.5]	87.2 [51.2,206.7]	62.5 [29.2,141.1]
	Width (μm)	0.0	–	–	4.3 [2.7,10.8]	11.1 [4.2,50.1]	11.5 [4.8,25.5]	6.7 [3.7,12.2]
	Depth (μm)	0.0	–	–	15.0 [7.5,40.0]	25.0 [16.9,60.6]	25.0 [12.5,63.8]	17.5 [10.0,35.0]
	Angle ($^\circ$)	0.0	–	–	45.0 [29.0,52.0]	35.0 [0.0,45.0]	40.0 [2.5,55.5]	44.0 [0.0,60.0]
PC	Density (#/μm^2)	0.0	4.4 [2.2,6.3]	4.9 [3.4,6.8]	5.7 [2.0,7.9]	2.0 [1.1,3.5]	2.7 [2.6,4.4]	2.6 [1.6,5.3]
	Length (μm)	0.0	50.6 [33.7,79.0]	57.8 [38.4,106.3]	67.4 [37.1,216.5]	140.0 [68.8,417.0]	88.2 [45.7,299.4]	64.1 [24.5,160.6]
	Width (μm)	0.0	4.7 [3.3,7.8]	4.1 [2.9,7.2]	6.5 [3.8,31.7]	18.6 [4.8,63.0]	17.7 [7.1,59.3]	4.1 [2.1,16.2]
	Depth (μm)	0.0	7.5 [5.0,15.0]	10.0 [7.5,15.0]	17.5 [10.0,45.0]	32.5 [12.5,95.6]	17.6 [12.5,55.0]	12.5 [7.5,27.5]
	Angle ($^\circ$)	0.0	35.0 [19.0,60.0]	54.0 [35.5,67.0]	45.0 [28.0,46.5]	30.0 [0.0,45.0]	37.5 [2.0,52.0]	42.0 [24.0,50.0]

Appendix B

In Table II we summarize our statistical findings (*P*-values and *F*-values).

Table II
Summary of statistical *p*-values and *F*-values via ANOVA with significant differences ($P < 0.05$) in bold and highlighted. Init. = Initiation; Prop. = Propagation; Cycl. Comp. = Cyclic Compression. Degrees of freedom (*df*): initiation columns *df* = 83; propagation columns *df* = 234.

Fixed Effect		Density (#/μm^2)		Length (μm)		Width (μm)		Depth (μm)		Angle (°)	
		Init.	Prop.	Init.	Prop.	Init.	Prop.	Init.	Prop.	Init.	Prop.
Condyle	*P*	0.782	–	0.733	0.490	0.729	0.680	0.274	0.976	0.864	0.907
	F	0.08	–	0.12	0.48	0.12	0.17	1.21	0.00	0.03	0.01
Impact	*P*	0.877	–	0.365	0.930	**0.021**	0.478	0.153	0.818	0.737	0.718
	F	0.02	–	0.83	0.01	5.51	0.51	2.08	0.05	0.11	0.13
Cycl. Comp.	*P*	**0.053**	–	0.570	0.886	0.745	0.754	0.916	0.415	0.871	0.559
	F	3.84	–	0.33	0.02	0.11	0.10	0.01	0.67	0.03	0.34
Impact × Cycl. Comp.	*P*	0.151	–	0.086	**0.018**	**0.031**	**0.025**	0.105	0.498	**0.012**	**0.020**
	F	2.1	–	3.03	5.64	4.83	5.13	2.69	0.46	6.67	5.50
Phase	*P*	0.596	–	0.620	**<.0001**	0.137	**<.0001**	0.533	0.745	0.965	0.444
	F	0.28	–	0.25	16.5	2.25	173.1	0.39	0.11	0.00	0.59
Phase × Impact	*P*	0.396	–	0.641	0.205	0.236	0.047	0.705	0.666	0.937	0.780
	F	0.73	–	0.22	1.61	1.43	4.16	0.14	0.19	0.01	0.08
Phase × Cycl. Comp.	*P*	0.474	–	0.947	0.234	0.695	0.239	0.078	**0.014**	0.304	0.258
	F	0.52	–	0.00	1.20	0.15	1.39	3.20	6.10	1.07	1.28
Thickness	*P*	0.257	–	0.198	0.467	**0.035**	0.189	0.506	0.958	0.147	0.361
	F	1.3	–	1.68	0.53	4.59	1.74	0.45	0.00	2.14	0.84
Thickness × Impact	*P*	0.8175	–	0.180	0.782	**0.007**	0.551	0.067	0.854	0.972	0.736
	F	0.05	–	1.83	0.08	7.73	0.36	3.44	0.06	0.00	0.11

Appendix C

In Fig. 6 we show the normalized probability of finding microcracks at given lengths, widths, depths, and angles relative to the local split-line direction in the PI and post-cyclic compression phases of our experiment under the three different impact treatments (none, low, high), and thereafter the three different cyclic compression treatments (none, low, high).

References

1. Kaleem B, Maier F, Drissi H, Pierce DM. Low-energy impact of human cartilage: predictors for microcracking the network of collagen. Osteoarthritis Cartilage 2017;25:544–53.
2. Lawrence RC, Felson DT, Helmick CG, Arnold LM, Choi H, Deyo RA, *et al.* National Arthritis Data Workgroup. Estimates of the prevalence of arthritis and other rheumatic conditions in the United States: Part II. Arthritis Rheum 2008;58:26–35.
3. Peña E, Pérez del Palomar A, Calvo B, Martínez MA, Doblaré M. Computational modelling of diarthrodial joints. Physiological, pathological and pos-surgery simulations. Arch Comput Methods Eng 2007;14:47–91.
4. Buckwalter JA, Mankin HJ, Grodzinsky AJ. Articular cartilage and osteoarthritis. Instr Course Lect 2005;54:465–80.
5. Workman J, Thambyah A, Broom N. The influence of early degenerative changes on the vulnerability of articular cartilage to impact-induced injury. Clin Biomech 2017;43:40–9.
6. Burr DB, Martin RB, Schaffler MB, Radin EL. Bone remodeling in response to in vivo fatigue microdamage. J Biomech 1985;18:189–200.
7. Zioupos P, Wang XT, Currey JD. The accumulation of fatigue microdamage in human cortical bone of two different ages in vitro. Clin Biomech 1996;11:365–75.
8. Martin RB. Is all cortical bone remodeling initiated by microdamage? Bone 2002;30:8–13.
9. Landrigan MD, Li J, Turnbull TL, Burr DB, Niebur GL, Roeder RK. Contrast-enhanced micro-computed tomography of fatigue microdamage accumulation in human cortical bone. Bone 2011;48:443–50.
10. Agcaoglu S, Akkus O. Acoustic emission based monitoring of the microdamage evolution during fatigue of human cortical bone. J Biomech Eng 2013;135. 081005–081005–8.
11. Repo RU, Finlay JB. Survival of articular cartilage after controlled impact. J Bone Jt. Surg 1977;59:1–2.
12. Finlay JB, Repo RU. Cartilage impact in vitro: effect of bone and cement. J Biomech 1978;11. 379,387–385,388.
13. Atkinson TS, Haut RC, Altiero NJ. An investigation of biphasic failure criteria for impact-induced fissuring of articular cartilage. J Biomech Eng 1998;120:536–7.
14. Duda GN, Eilers M, Loh L, Hoffman JE, Kääb M, Schaser K. Chondrocyte death precedes structural damage in blunt impact trauma. Clin Orthop Relat Res 2001;393:302–9.
15. Clarke IC. Surface characteristics of human articular cartilage—a scanning electron microscope study. J Anat 1971;108:23–30.
16. Clarke LC. The microevaluation of articular surface contours. Ann Biomed Eng 1972;1:31–43.
17. Kaplan JT, Neu CP, Drissi H, Emery NC, Pierce DM. Cyclic loading of human articular cartilage: the transition from compaction to fatigue. J Mech Behav Biomed Mater 2017;65:734–42.
18. Novakofski KD, Williams RM, Fortier LA, Mohammed HO, Zipfel WR, Bonassar LJ. Identification of cartilage injury using quantitative multiphoton microscopy. Osteoarthritis Cartilage 2014;22:355–62.
19. Mansfield JC, Bell JS, Winlove CP. The micromechanics of the superficial zone of articular cartilage. Osteoarthritis Cartilage 2015;23:1806–16.
20. Kiyomatsu H, Oshima Y, Saitou T, Miyazaki T, Hikita A, Miura H, *et al.* Quantitative SHG imaging in osteoarthritis

model mice, implying a diagnostic application. Biomed Opt Express 2015;6:405–20.
21. Kumar R, Grønhaug KM, Davies CL, Drogset JO, Lilledahl MB. Nonlinear optical microscopy of early stage (ICRS Grade-I) osteoarthritic human cartilage. Biomed Opt Express 2015;6:1895–903.
22. Hoeger WWK, Bond L, Ransdell L, Shimon JM, Merugu S. One-mile step count at walking and running speeds. ACSM's Health & Fit J 2008;12:14–9.
23. Athanasiou KA, Rosenwasser MP, Buckwalter JA, Malinin TI, Mow VC. Interspecies comparisons of in situ intrinsic mechanical properties of distal femoral cartilage. J Orthop Res 1991;9:330–40.
24. Neu CP, Khalafi A, Komvopoulos K, Schmid TM, Reddi AH. Mechanotransduction of bovine articular cartilage superficial zone protein by transforming growth factor β signaling. Arthritis Rheum 2007;56:3706–14.
25. Schindelin J, Arganda-Carreras I, Frise E. Fiji: an open-source platform for biological-image analysis. Nat Methods 2012;9:676–82.
26. Szarko M, Muldrew K, Bertram JEA. Freeze-thaw treatment effects on the dynamic mechanical properties of articular cartilage. BMC Muscoskelet Disord 2010;11:1–8.
27. Mow VC, Wang CC, Hung CT. The extracellular matrix, instertitial fluid and ion as a mechanical signal transducer in articular cartilage. Osteoarthritis Cartilage 1999;7:41–58.
28. Korhonen RK, Laasanen MS, Töyräs J, Rieppo J, Hirvonen J, Helminen HJ, *et al*. Comparison of the equilibrium response of articular cartilage in unconfined compression, confined compression and indentation. J Biomech 2002;35:903–9.
29. Park S, Hung CT, Ateshian GA. Mechanical response of bovine articular cartilage under dynamic unconfined compression loading at physiological stress levels. Osteoarthritis Cartilage 2004;12:65–73.
30. Zhang L, Miramini S, Smith DW, Gardiner BS, Grodzinsky AJ. Time evolution of deformation in a human cartilage under cyclic loading. Ann Biomed Eng 2015;43:1166–77.
31. Liu F, Kozanek M, Hosseini A, de Velde SKV, Gill TJ, Rubash HE, *et al*. *In vivo* tibiofemoral cartilage deformation during the stance phase of gait. J Biomech 2010;43:658–65.
32. Harkey MS, Blackburn JT, Davis H, Sierra-Arevalo L, Nissman D, Pietrosimone B. Ultrasonographic assessment of medial femoral cartilage deformation acutely following walking and running. Osteoarthritis Cartilage 2017;25:907–13.
33. Preibisch S, Saalfeld S, Tomancak P. Globally optimal stitching of tiled 3D microscopic image acquisitions. Bioinformatics 2009;25:1463–5.
34. He B, Wu JP, Kirk TB, Carrino JA, Xiang C, Xu J. High-resolution measurements of the multilayer ultra-structure of articular cartilage and their translational potential. Arthritis Res Ther 2014;16:205.
35. McHugh ML. Interrater reliability: the kappa statistic. Biochem Med 2012;22:276–82.
36. Tavakoli AS, Cai B, Snyder R, Huynh N. Calculating multi-rater observation agreement in health care research using the SAS kappa statistic. In: Proceedings of the SAS Global Forum 2012 2012;vols. 201–2012:1–11. Orlando, Florida.
37. Gelse K, P'oschl E, Aigner T. Collagens - structure, function, and biosynthesis. Adv Drug Deliv Rev 2003;55:1531–46.
38. von der Mark K. Structure, biosynthesis and gene regulation of collagens in cartilage and bone. In: Seibel MJ, Robins SP, Bilezikian JP, Eds. Dynamics of Bone and Cartilage Metabolism. Orlando: Academic Press; 1999:3–29.
39. Henzgen S, Petrow PK, Thoss K, Braur R. Degradation of articular cartilage during the progressionof antigen-induced arthritis in mice: a scanning and transmission electron microscope study. Exp Toxicol Pathol 1996;48:255–63.
40. Andriacchi TP, Mündermann A, Smith RL, Alexander EJ, Dyrby CO, Koo S. A framework for the in vivo pathomechanics of osteoarthritis at the knee. Ann Biomed Eng 2004;32:447–57.
41. Lewis JL, Johnson SL. Collagen architecture and failure processes in bovine patellar cartilage. J Anat 2001;199:483–92.
42. Bonitsky C, McGann ME, Selep MJ, Ovaert TC, Trippel SB, Wagner DR. Genipin crosslinking decreases the mechanical wear and biochemical degradation of impacted cartilage in vitro. J Orthop Res 2017;35:558–65.
43. Kafka V. Surface fissures in articular cartilage: new concepts, hypotheses and modeling. Clin Biomech 2002;17:73–80.
44. Santos S, Maier F, Pierce DM. Anisotropy and inter-condyle heterogeneity of cartilage under large-strain shear. J Biomech 2017;52:74–82.
45. Greene G, Zappone B, Soderman O, Topgaard D, Rata G, Zeng H, *et al*. Anisotropic dynamic changes in the pore network structure, fluid diffusion, and fluid flow in articular cartilage under compression. Biomaterials 2010;31:3117–28.
46. Brown CP, Houle MA, Chen M, Price AJ, Légaré F. Damage initiation and progression in the cartilage surface probed by nonlinear optical microscopy. J Mech Behav Biomed Mater 2012;5(1):62–70.
47. Moos V, Fickert S, Muller B, Weber U, Sieper J. Immunohistological analysis of cytokine expression in human osteoarthritic and healthy cartilage. J Rheumatol 1999;26:870–9.
48. Tetlow LC, Adlam DJ, Woolley DE. Matrix metalloproteinase and proinflammatory cytokine production by chondrocytes of human osteoarthritic cartilage: associations with degenerative changes. Arthritis Rheum 2001;44:585–94.
49. Schueller-Weidekamm C, Shueller G, Uffmann M, Bader TR. Does marathon running cause acute lesions of the knee? Evaluation with magnetic resonance imaging. Eur Radiol 2006;16:2179–85.
50. Regatte RR, Akella SVS, Lonner JH, Kneeland JB, Reddy R. T1ρ relaxation mapping in human osteoarthritis (OA) cartilage: comparison of T1ρ with T2. Magn Reson Imaging 2006;23:547–53.